www.czasopisma.pan.pl PAN www.journals.pan.pl
Chemical and Process Engineering 2021, 42 (4), 349–368
DOI: 10.24425/cpe.2021.138935

The effect of capillary pumping on the course of cleaning porous materials containing liquid contaminants using supercritical fluids – A pore network study

Jan Krzysztoforski[1*], Karim Khayrat[2], Marek Henczka[1], Patrick Jenny[2]

[1]Warsaw University of Technology, Faculty of Chemical and Process Engineering, Waryńskiego 1, 00-645 Warsaw, Poland
[2]ETH Zurich, Institute of Fluid Dynamics, Sonneggstrasse 3, 8092 Zurich, Switzerland

The role of capillary pumping on the course of cleaning porous materials containing liquid contaminants using supercritical fluids was investigated numerically. As a specific process to be modelled, cleaning of porous membranes, contaminated with soybean oil, using supercritical carbon dioxide as the cleaning fluid (solvent) was considered. A 3D pore-network model, developed as an extension of a 2D drying model, was used for performing pore scale simulations. The influence of various process parameters, including the coordination number of the pore network, the computational domain size, and the external flow mass transfer resistance, on the strength of the capillary pumping effect was investigated. The capillary pumping effect increases with increasing domain size and decreasing external flow mass transfer resistance. For low coordination numbers of the pore network, the capillary pumping effect is not noticeable at macro scale, while for high coordination numbers, the opposite trend is observed – capillary pumping may influence the process at macro scale. In the investigated system, the coordination number of the pore network seems to be low, as no capillary pumping effects were observed at macro scale during experimental investigation and macro-scale modelling of the membrane cleaning process.

Keywords: porous material, supercritical fluid, mathematical modelling, cleaning, capillary pumping

1. INTRODUCTION

In many industrial processes, supercritical fluids (SCFs) have become a feasible alternative to liquid organic solvents. This is due to the unique properties of SCFs, combining favourable characteristics of liquids and gases. Among all SCFs, supercritical carbon dioxide is the most popular one, thanks to relatively moderate critical parameters, a high degree of process safety, low cost and its ability to dissolve numerous substances. Hence, supercritical carbon dioxide meets the principles of green chemistry (Anastas and Warner, 1998) and green engineering (Anastas and Zimmerman, 2003) to a substantially higher degree than traditional organic solvents.

* Corresponding author, e-mail: jan.krzysztoforski@pw.edu.pl

One class of processes, in which SCFs are successfully applied, are processes for cleaning porous materials from liquid or solid contaminants, using supercritical fluids as cleaning media. The rate of the cleaning process depends on numerous parameters, such as the morphology of the porous material, the physical properties of the supercritical fluid, process conditions, the type of the contaminant and thermodynamic equilibria (limited or full miscibility of contaminant and solvent), the geometry and the hydrodynamics of the cleaning vessel, and – for liquid contaminants – possible capillary effects, as for low values of the capillary number Ca (the force ratio of drag/surface tension), flow through porous media is controlled by capillary forces. Examples of cleaning processes for porous materials, involving SCFs as cleaning media, include, among others, purification of cork stopper (Taylor et al., 2000), drying of alcogels (Özbakır and Erkey, 2015), soil remediation (Cocero et al., 2000), and cleaning of microfiltration membranes (Krzysztoforski et al., 2013; Michałek et al., 2015).

SCFs can be applied as cleaning media in the process of manufacturing microfiltration membranes by the Temperature Induced Phase Separation method (Berghmans et al., 1996), replacing liquid organic solvents. In this method, the pores of newly produced microfiltration membranes are usually filled with a liquid contaminant (oil), which has to be removed prior to membrane operation. The specific case of cleaning polypropylene microfiltration membranes, contaminated with a model contaminant (soybean oil), using pure $scCO_2$ or $scCO_2$ with minor amounts of organic solvents, was studied extensively. It was shown that the addition of minor amounts of organic solvents to $scCO_2$ enhanced the process rate (Krzysztoforski et al., 2013; Michałek et al., 2015). Moreover, it was proven that $scCO_2$ does not deteriorate the material properties of the polypropylene microfiltration membrane (Tarabasz et al., 2016). The effect of various process parameters on the course of the membrane cleaning process was studied experimentally (Krzysztoforski and Henczka, 2018), and a mathematical model of the process, suitable for CFD simulations in macro scale, was developed (Krzysztoforski et al., 2018). The mathematical model is based on the Volume of Fluid multiphase model and utilizes the continuum approach for modelling the porous zone. Moreover, it implies that there is a sharp phase boundary between the contaminant and solvent inside the porous material in macro scale and that capillary effects do not influence the process in macro scale. The simulation results obtained with this model were consistent with the experimental results. However, in the macro-scale model, the capillary effects are neglected and the process is not simulated at the scale of individual pores (instead, the continuum approach was used), which is the main limitation of this approach. On the other hand, if the Ca number is low (which was the case in the investigated process), capillary forces may lead – depending on many different factors – to the development of an "unsharp" phase boundary, namely an intermediate zone, in which neighbouring pores containing either the contaminant or the solvent exist. This would, in turn, enhance the process rate due to a phenomenon known as "capillary pumping", which is a viscous flow of the wetting phase induced by capillarity, leading to a significant increase of the wetting phase mass flux towards the outer surface of the porous body (see e.g. Tsimpanogiannis et al., 1999).

An alternative modelling approach is to model transport phenomena in porous materials in pore scale by explicit mathematical formulation of phenomena occurring in pore networks consisting of individual pores linked to one another via tubes. Pore scale modelling enables to get a detailed insight in the process and to assess the role of capillary effects, which – in fact – occur in individual pores and/or tubes. The main limitation of pore-network models is that they are computationally demanding and can be applied only for simulations of local transport phenomena. Nevertheless, the pore scale modelling results can be used for numerical investigation of the process and/or for calibration of macro-scale models, which can be applied to simulate the whole apparatus. Pore-network models have been applied successfully for such processes as drying (e.g., Yiotis et al., 2001) and geological processes (e.g. Al Dhahli et al., 2012; Liu et al., 2020; Rabbani et al., 2020; Wang et al., 2020 and Xu et al., 2011).

Therefore, the motivation of this work was to apply the pore-network modelling approach to investigate the membrane cleaning process described above at the pore scale in order to assess the role of the capillary

forces, and especially capillary pumping, on the course of the process. Hence, the aims of this work are formulated as follows:

- numerical investigation of the membrane cleaning process at pore scale;
- estimation of the capillary effects, including capillary pumping;
- determination of the dependence between the morphology of the porous material and the intensity of the capillary effects; and
- assessment of the impact of pore-scale effects on the course of the process at macro scale.

Although the numerical investigation was carried out for a specific process (namely, the membrane cleaning process, as described by Krzysztoforski and Henczka (2018) and Krzysztoforski et al. (2018)), the considerations presented herein are of a general nature and the conclusions may be valid – to a certain extent – for other cleaning processes involving porous materials, liquid contaminants and supercritical fluids as cleaning media, characterized by low values of the Ca number.

2. MATHEMATICAL MODEL

2.1. Assumptions for model development

The aim of pore-scale modelling in this work is to identify the pore-scale capillary effects in the membrane cleaning process using a simplified model, in which other phenomena are neglected. The assumptions for the development of a pore-scale model of the membrane cleaning process are listed below:

- The computational domain is a pore network structure with adjustable properties (2D/3D, domain size, coordination number of the pores, etc.).
- In the system, two fluid phases exist:
  1) the oil phase (wetting phase – soybean oil);
  2) the solvent phase (non-wetting phase – scCO_2).
- The process is isothermal.
- The oil phase composition is constant in the domain, i.e., a) the dissolution of CO_2 in the oil phase is neglected or b) complete saturation of the oil phase with CO_2 is assumed at the beginning of the simulation. In the presented pore-scale model, both versions of this assumption can be regarded as equivalent. Therefore, the approach a) is selected for the development of the model, as it is simpler for model formulation and interpretation.
- The solvent phase consists of two components (soybean oil is moderately soluble in the solvent phase – analogically to the macro-scale model of the membrane cleaning process by Krzysztoforski et al. (2018)).
- The Stefan flow in the porous material is negligible, i.e., no convective mass transfer occurs in the solvent phase (due to the low solubility of soybean oil in the solvent phase and a small difference in the densities of the phases).
- Steady state diffusion of soybean oil in the solvent phase occurs (due to low solubility of soybean oil in the solvent phase, diffusion reaches steady state before a substantial change of the phase boundary location occurs).
- The oil phase gradually dissolves in the solvent phase and its dissolution is controlled by diffusive mass transfer (analogically to the macro-scale model of the membrane cleaning process).
- Capillary effects dominate in the process (low values of the Capillary and the Bond number).

2.2. Model formulation

The algorithm of the pore-scale model is based on the pore network model developed by Yiotis et al. (2001), who proposed a model for 2D numerical simulation of drying processes. The major differences between the above-mentioned pore network model and the algorithm presented in this work include adaptation of the algorithm for handling 3D domains with varying coordination numbers of the pore network, as well as the assumption that the mass transfer in the solvent phase occurs only due to diffusion (convection term is neglected) and that diffusion reaches a quasi-steady state. The soybean oil concentration in the solvent phase is described by the dimensionless concentration C, which is defined as

$$C = \frac{c}{s} \tag{1}$$

where c is the concentration of soybean oil, and s is the solubility of soybean oil in the solvent phase.

The pore network consists of pores and tubes, which connect neighbouring pores. Four different types of pores, i.e.:

L – a pore completely filled with the oil phase,

A – a pore containing the oil phase, but being gradually emptied, as the solvent phase enters this pore through an adjacent i tube; the soybean oil concentration C in the solvent phase is equal to 1 (full saturation),

S – a pore filled with the solvent phase, and connected to at least one tube containing the phase boundary; therefore, the soybean oil concentration C in the solvent phase is also equal to 1 (full saturation),

G – a pore completely filled with the solvent phase and not connected to any tubes containing the phase boundary (b tubes); in general, in such a pore, the oil concentration C in the solvent phase can be lower than 1,

and four types of tubes, i.e.:

l – a tube completely filled with the solvent phase. It connects two L pores or an A pore and a L pore,

b – a tube containing the phase boundary with a meniscus (both phases are present); it is a potential candidate for solvent invasion and it connects an S pore with an L or an A pore,

i – a tube filled with the solvent phase; it leads to the current A pore of the cluster,

g – a tube filled with the solvent phase; it connects two G pores or two S pores or a G pore and an S pore,

which correspond to different states, can be distinguished. Both pores and tubes are of random sizes. The pores have non-zero volumes available for the fluid phases and do not cause any mass transfer resistance. On the contrary, the tubes do not have formal volumes available for the fluid phases (the fluid phases in a tube linking two pores are attributed to these two pores), but they cause mass transfer resistance. This mass transfer resistance results from the geometry of a tube, which is defined by its radius r and length l. In the investigated pore network, two phases are present in the porous network: the oil phase (soybean oil forming the wetting phase, which is moderately soluble in $scCO_2$) and the solvent phase ($scCO_2$ forming the non-wetting phase). Carbon dioxide is assumed to be insoluble in soybean oil; however, although the assumption of complete saturation of the soybean oil phase with CO_2 at the start of the process – as was observed in macro-scale simulations (Krzysztoforski et al., 2018) – is an equivalent approach and leads to the same results. Dissolution of the oil phase in the solvent phase occurs at the phase boundary. The scalar field C in the solvent phase is the dimensionless concentration of soybean oil in the solvent phase (analogically to the C scalar in the macro-scale model). The dissolution rate is controlled by the diffusive mass transfer of soybean oil in the solvent phase (convective mass transfer is neglected). In the domain, one or more clusters ("islands" – which are sets of pores connected to each other by the oil phase) may exist. Each cluster undergoes dissolution in the solvent phase through all the external tubes of the cluster, which contain the phase boundary between the oil phase and the solvent phase. However, due to capillary forces, which dominate in the process, the menisci in the tubes containing the phase boundary are stationary. In order to allow this and to meet the mass balance, convective flow inside the cluster – referred to as the capillary pumping – takes place from one specific pore (the A pore) of the cluster and is directed to all

boundary tubes. Each cluster has an A pore, which was subject to an invasion of the solvent phase through a boundary tube with the largest diameter in the cluster. Due to the dissolution process, the oil phase within the A pore is removed and the A pore becomes "empty" (i.e., completely filled with the solvent phase). Then, a new A pore is selected by searching the new largest boundary tube of the cluster, which is characterized by the weakest capillary forces and is, hence, prone to invasion of the solvent phase. The convective flow within the oil phase is not modelled explicitly. The algorithm of the pore-scale model is briefly described in Table 1 and a more detailed description can be found in the Appendix.

Table 1. Algorithm of the pore-scale model

Initial stage In the initial phase, the computational domain is prepared and initial conditions are set.
Time loop 1. **Cluster identification step** – Among all the A and L pores in the domain, separate clusters are identified. Active pores are assigned to the clusters, if available (during the first iteration, only one cluster – without any A pores – is present in the domain). 2. **Invasion step** – For all the clusters that do not have active pores, new active pores are identified by searching for the b tube with the largest radius (and therefore, the lowest capillary pressure) among all b tubes of a given cluster. The tube becomes an i tube, and the destination pore becomes an A pore. 3. **Diffusion step** – The soybean oil concentration distribution in the solvent phase ($scCO_2$) is calculated for steady-state diffusion, using the G pores at the domain boundary and A/S pores as Dirichlet boundary conditions, resulting in the soybean oil concentration C field in the solvent phase. 4. **Flux step** – The mass fluxes of dissolution are calculated for all clusters, based on the concentration distribution of the oil in the solvent phase. The cleaning time values needed for emptying the active pores of all of the clusters are calculated. The minimum value is chosen as the time step. The active pore corresponding to this time step becomes empty. The rest of A pores in the domain (corresponding to the remaining clusters) remain partially empty. 5. **Update step –** The status of the former A pore, the former i tube and the neighbour tubes and pores are updated. The time loop is repeated until no A and L pores are present in the domain.
Final stage Simulation results are saved to text files.

In Figure 1, three iterations (I–III) of the pore-scale algorithm are presented for an exemplary, simple 2D domain. During each iteration, one L pore becomes an A pore due to invasion through a single b tube, which becomes an i tube. The sequence of A pores depends on the tube diameter distribution in the domain. The b tubes and L pores, which will undergo invasion during the next iteration, are highlighted. The first iteration is shown in more detail (Ia–Ic):

- Step Ia – All clusters in the domain are identified (in this example, one cluster is present). The b tubes of the cluster are scanned and the candidate for invasion (for becoming an i tube) is found – it is the b tube with the largest diameter. The i tube points to the new A pore (Steps 1–2 of the algorithm).
- Step Ib – The concentration field C of soybean oil in the solvent phase is computed for steady-state diffusion. Then, the mass flux from the cluster is calculated. Based on the mass flux, the cleaning time needed for emptying the active pore is calculated. While the simulation advances with this time step, the A pore becomes empty (Steps 3–4 of the algorithm).

- Step Ic – The status of the pores and tubes involved in the last invasion is updated. The A pore becomes an S pore, the i tube becomes a g tube, etc. (Step 5 of the algorithm). The cluster contains L pores only – it is ready for the next invasion (in Iteration II).

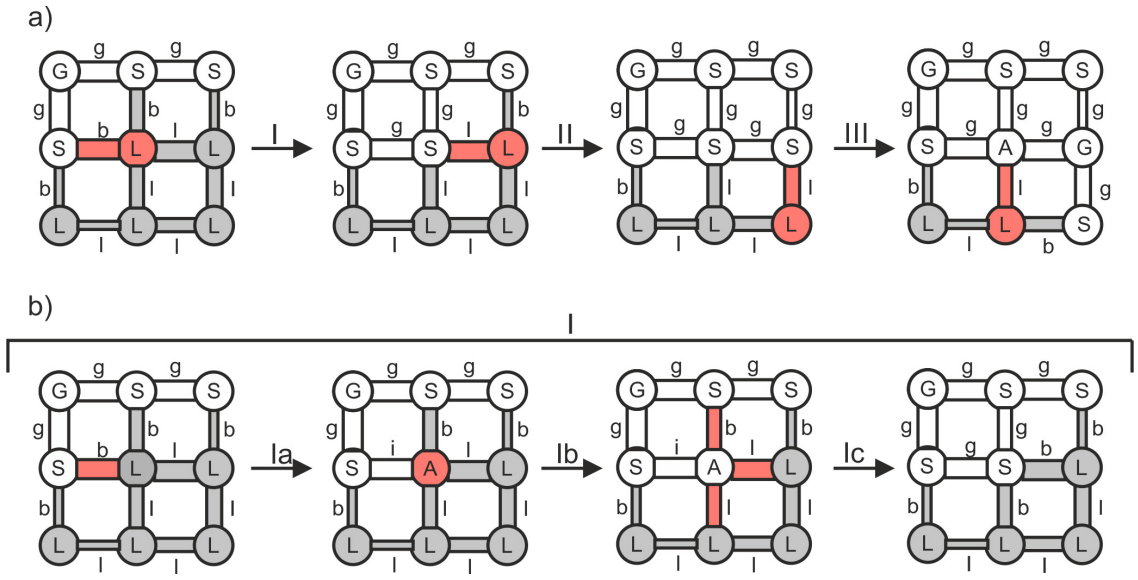

Fig. 1. Scheme of the pore-scale model algorithm: a) three iterations of the algorithm, and b) the first iteration in detail

2.3. Numerical implementation

The numerical implementation of the algorithm was performed in Python 2.6 programming language. For implementation, a pore network model framework developed by Khayrat and Jenny (2016, 2017) was used. The framework consists of basic tools and components such as pore network generators, numerical algorithms for cluster identification, linear system solvers, etc. In this work, the known drying algorithm was adapted to porous membrane cleaning and implemented into the pore network model framework. The numerical simulations were performed on a PC (quad-core Intel processor) with Linux OS (Ubuntu 12.04 LTS).

2.4. Test cases for numerical investigation

In Figure 2, initial and boundary conditions for the pore-scale simulations are shown. The first row is the "outlet" of the system and the interface with the free solvent flow around the porous body. This row contains G pores (solvent phase) with the Dirichlet boundary condition ($C = 0$), i.e., the mass transfer resistance in the bulk of the solvent flowing around the porous material is neglected. The second row contains S pores and the remaining pores in the domain are L pores (containing the oil phase). The phase boundary is placed between the second and the third row. The L pores change gradually into G pores, as the process advances. The simulation stops when the last L pore becomes an A pore and finally a G pore. A periodic boundary condition is set for the plane perpendicular to the x direction. For 3D simulations, the periodic boundary condition is also set for the plane perpendicular to the z direction.

The basic geometry is a square for 2D domains and a cube for 3D domains. The domain size is characterized by N – the number of pores in x direction (10 and 20 for 2D simulations and 10 for 3D simulations). Different shapes of the domains were tested by varying the number of pores in y direction (the direction of mass transfer). A shape factor β (equal to 1, 2, 4, 8, or 16) was introduced, and the dimensions of the domain were $N_x = N$, $N_y = \beta N$, and $N_z = 1$ for 2D simulations and $N_x = N$, $N_y = \beta N$, and $N_z = N$ for 3D simulations.

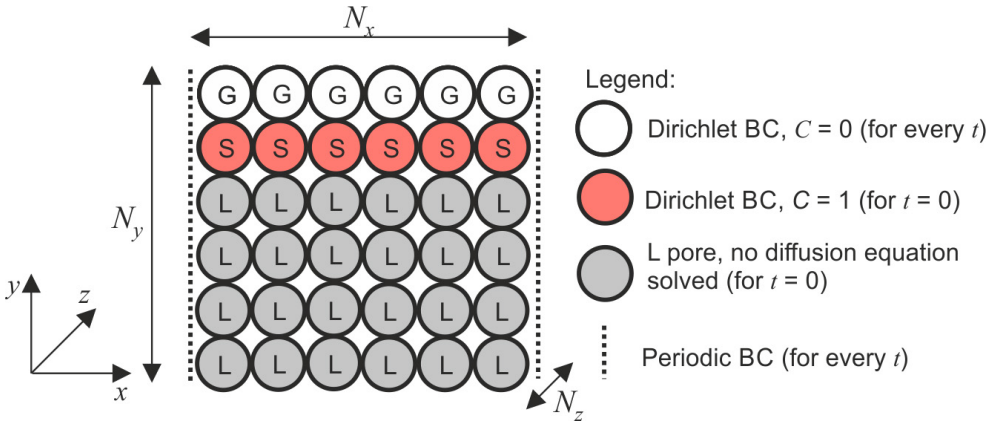

Fig. 2. Initial and boundary conditions for the pore-scale model simulations

Standard coordination numbers n_{coord} of the 2D and 3D pore networks are 4 and 6, respectively. For 3D simulations, higher coordination numbers were tested as well (n_{coord} = 8, 10, or 12). Both the mean pore diameter and mean tube length were set to 1 μm (with a normal distribution), while the mean tube diameter was set to 0.2 μm (with a normal distribution). As the simulation results were analysed using dimensionless, relative quantities by comparison with results obtained from simulations without capillary effects, the diffusivity D and solubility S were set to 1.

In Table 2, the parameters used in the pore-scale simulations are summarized.

Table 2. Simulation parameters for pore scale modelling

Parameter	Values
Pore network type	2D, 3D
Pore network size N	10, 20 (2D) 10 (3D)
Shape factor β	1, 2, 4, 8, 16 (2D) 1, 2, 4, 8 (3D)
Pore network dimensions	
N_x	N
N_y	βN
N_z	1 (2D) N (3D)
Coordination number n_{coord}	4 (2D) 6, 8, 10, 12 (3D)

3. RESULTS AND DISCUSSION

3.1. Course of the cleaning process

In this subsection, exemplary results from the pore-scale modelling are presented in order to illustrate and discuss the course of the membrane cleaning process at pore scale. In order to quantify the contribution of the capillary effects to the mass transfer intensification (leading to higher process rate), the analytical

solution of a simple 1D model of the membrane cleaning process, which does not include capillary effects, is used as a reference. This solution will be referred to as "ideal", while the results obtained using the complete pore-scale model will be marked as "pnm" (pore network modelling). In the "ideal" case, where the capillary forces are not present or neglected, the cleaning process occurs uniformly at the phase boundary. Thus, the phase boundary remains a parallel plane and moves deeper and deeper into the porous structure, as the process advances.

The process rate for the ideal case is given by the following equation:

$$\frac{\mathrm{d}\eta}{\mathrm{d}t} = \frac{1}{m}\frac{1}{A + B\eta} \tag{2}$$

where η is the cleaning efficiency, t the time, m the initial mass of oil in the domain, $A = \dfrac{1}{\dot{m}_{\mathrm{start}}}$ a constant describing the initial mass transfer resistance at $t = 0$, and $B = \dfrac{1}{\dot{m}_{\mathrm{end}}} - \dfrac{1}{\dot{m}_{\mathrm{start}}}$ a constant describing the mass transfer resistance contribution coming from the progress of the cleaning process. The mass fluxes $\dot{m}_{\mathrm{start}}$ and $\dot{m}_{\mathrm{end}}$ are obtained by solving steady state diffusion in the pore network for the initial conditions of the pore network model, as well as for a special state of the pore network, when all pores are filled with the solvent phase, and only the deepest layer of the pore network is fully saturated with soybean oil. Therefore, the mass transfer resistance grows linearly with the cleaning efficiency.

The solution of Eq. (2) yields:

$$t(\eta) = \frac{1}{m}\left(\frac{B}{2}\eta^2 + A\eta\right) \tag{3}$$

Therefore, the final cleaning time (at which $\eta = 1$) for the ideal case can be calculated from the equation

$$t_{\mathrm{id}} = t(1) = \frac{1}{m}\left(\frac{B}{2} + A\right) \tag{4}$$

The process acceleration factor X, which describes process intensification due to capillary pumping, is defined as

$$X = \frac{t_{\mathrm{id}}}{t_{\mathrm{pnm}}} \tag{5}$$

where t_{id} is the total cleaning time obtained for the ideal case, and t_{pnm} is the total cleaning time obtained from the pore-scale model.

Exemplary results are presented for two cases:

- Case I: 2D simulation, domain size 20×20 (observed acceleration factor: $X = 1.68$);
- Case II: 2D simulation, domain size 80×20 (observed acceleration factor: $X = 1.39$).

In Figure 3, the phase distribution and the soybean oil concentration C in the solvent phase are shown for Case I. In Figure 4, various parameters describing the course of the membrane cleaning process at pore scale are presented ("pnm" – results from pore-scale modelling, and "ideal" – results for the ideal case without capillary effects). In graph 4a, cleaning efficiency is plotted against the dimensionless time (normalized with the total cleaning time obtained from the pore-scale model). In graph 4b, the relative mass flux of dissolution (normalized with the initial mass flux) is plotted against the cleaning efficiency. In graph 4c, the number of clusters is plotted against the cleaning efficiency, and in graph 4d, the relative interfacial area (normalized with initial interfacial area) is plotted against the cleaning efficiency. In Figures 5 and 6, analogous results are shown for Case II.

In Figures 3 and 5, the course of the membrane cleaning process, including the evolution of the phase boundary and the concentration distribution, is depicted for the two test cases. At the beginning, a parallel

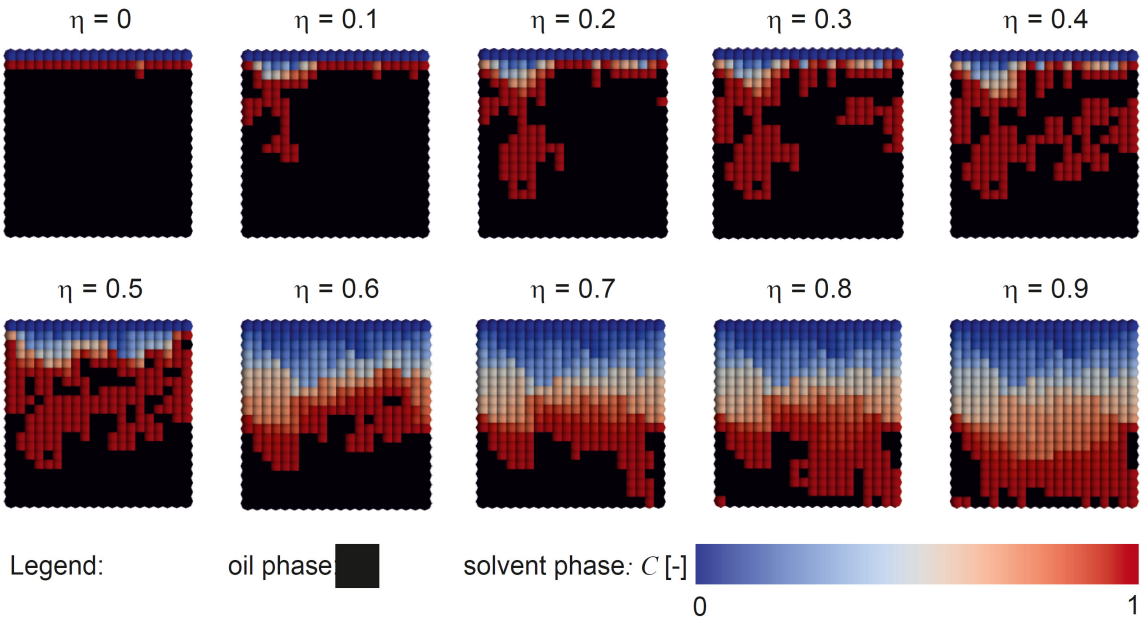

Fig. 3. Phase distribution and soybean oil concentration C in the solvent phase for a 2D simulation, Case I (20×20)

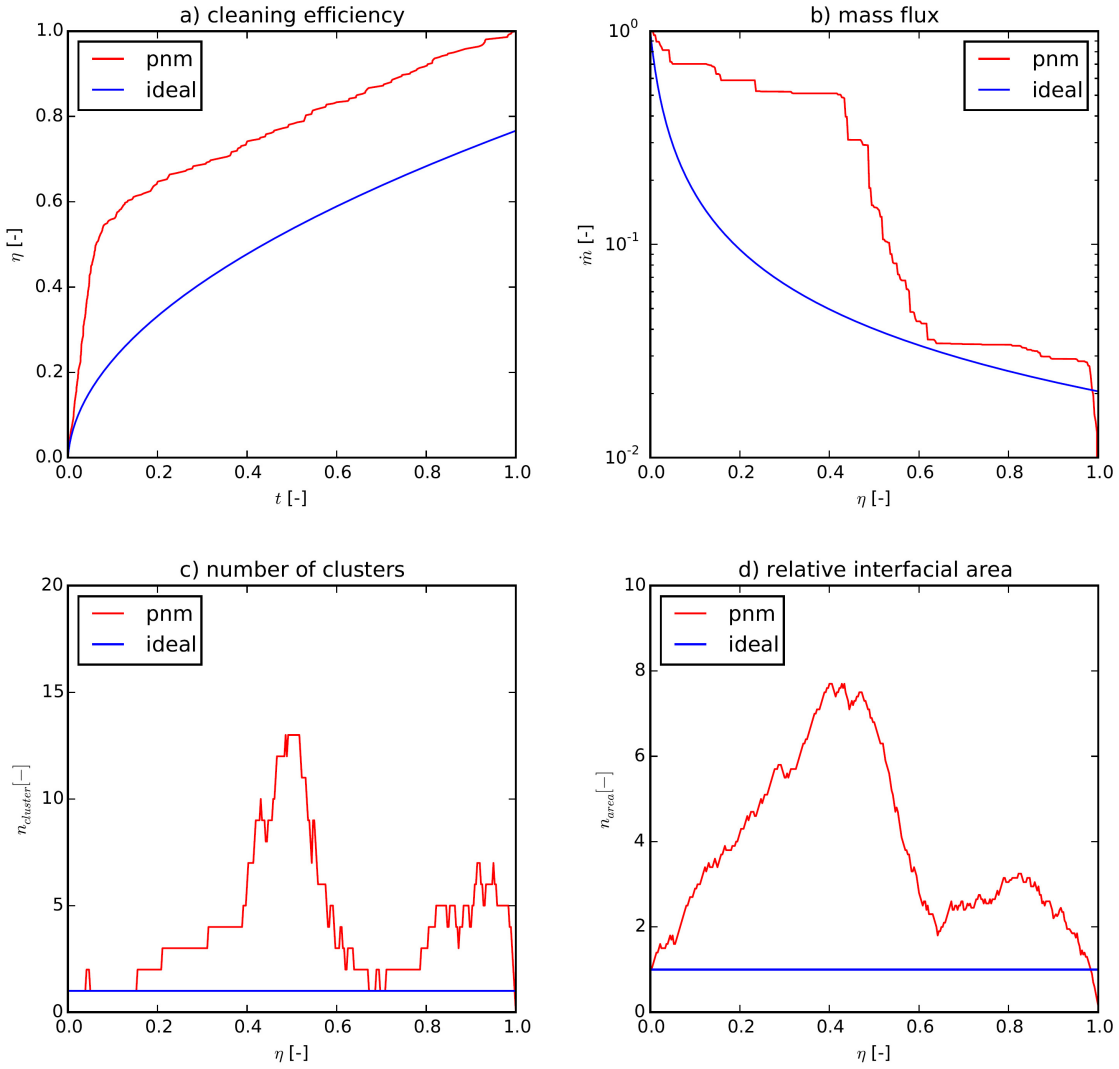

Fig. 4. Pore scale modelling results for a 2D simulation, Case I (20×20)

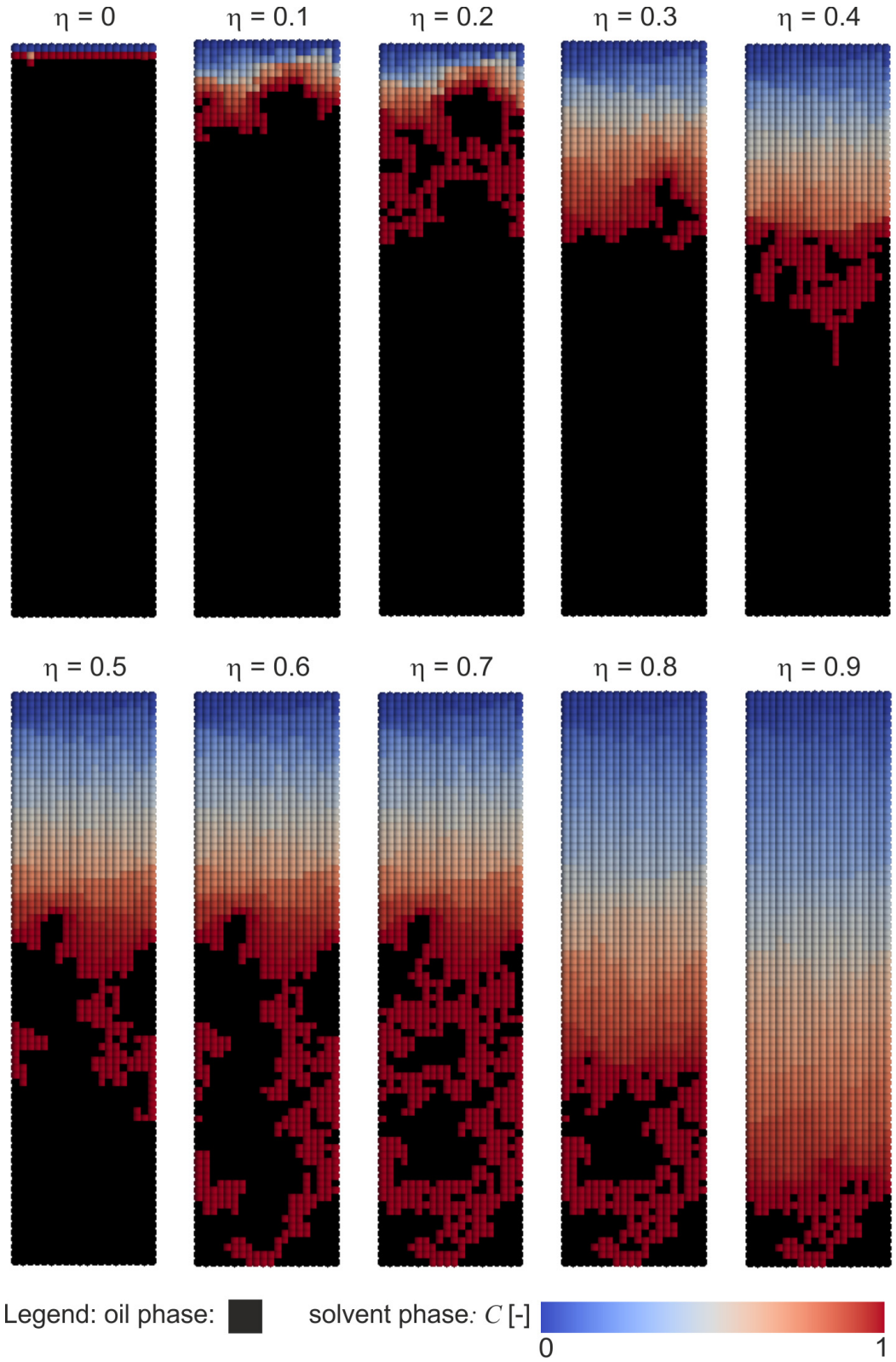

Fig. 5. Phase distribution and soybean oil concentration C in the solvent phase for a 2D simulation, Case II (20×80)

phase boundary is present in the system, but as the process advances, the phase boundary becomes irregular and an intermediate zone arises, in which both phases are present. The solvent phase deeply invades in the oil region, but the oil phase remains present close to the top border of the domain, which is the contact zone with the free solvent flow around the porous body. This provides a shorter diffusion path in the region where clusters ("islands") exist, as the solvent phase is fully saturated with soybean oil.

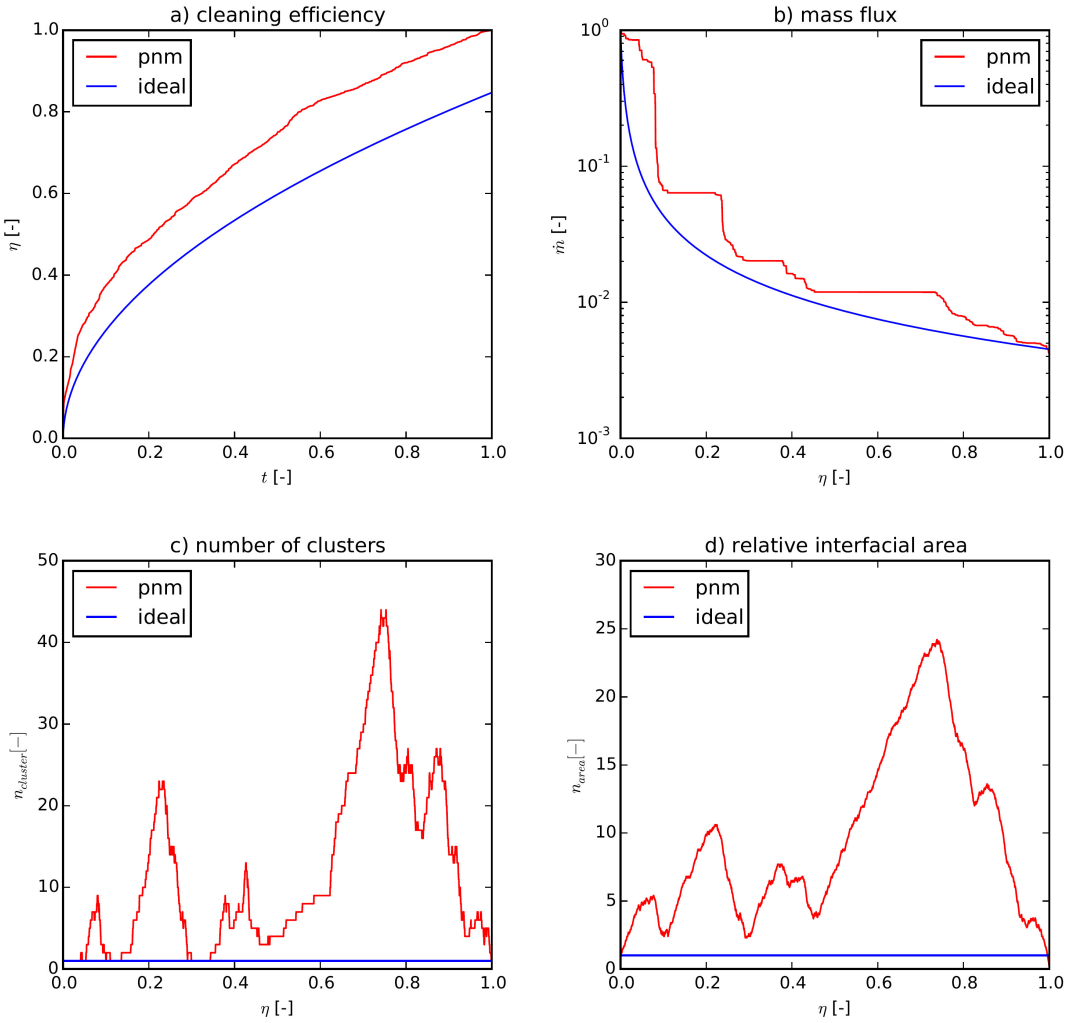

Fig. 6. Pore scale modelling results for a 2D simulation, Case II (20×80)

The aforementioned phenomenon of shortening the diffusion path is the capillary pumping effect, which leads to mass transfer intensification and higher process rates. The invasion process and emptying process of consecutive A pores might occur deep in the oil phase. However, there are still L pores located near the top domain boundary. The oil, which is removed from an active pore, flows through the connected L pores of a given cluster towards its boundary, where the actual dissolution process takes place (in the b tubes of the cluster, which contain the menisci of the phase boundary). This convective flow inside the oil phase is the reason for process acceleration. The number, shape and location of the clusters evolve in time. When small groups of pores become separated from the main cluster, they tend to undergo relatively fast dissolution, provided that they are not surrounded from all sides by other clusters.

In Figures 4 and 6, key parameters describing the course of the membrane cleaning process are plotted against dimensionless time t or cleaning efficiency η. In graphs 4a and 6a, the process rates obtained for the pore-scale model and the ideal case (no capillary forces) can be compared. Due to capillary pumping, the process is faster in the first case. In graphs 4b and 6b, the mass fluxes (being indicators of the current process rate) are plotted as a function of the cleaning efficiency. The difference between the "pnm" and "ideal" mass flux comes from the developed intermediate zone. If this zone shrinks, the process acceleration due to capillary pumping becomes weaker. For example, a rapid decrease of this difference can be observed in Figure 4 between $\eta = 0.5$ and $\eta = 0.6$. The reason behind this change is clearly visible in Figure 3, where many clusters disappeared between $\eta = 0.5$ and $\eta = 0.6$, which resulted in a longer diffusion path. In graphs 4c/6c and 4d/6d, the evolution of the number of clusters and the relative interfacial area is shown.

These two quantities oscillate and are strongly correlated. A sudden decrease of these quantities results also in a decrease of the process rate.

Both Case I and Case II show a similar behaviour of the investigated system and the same mass transfer intensification mechanism (capillary pumping). The main difference is the higher number of islands in Case II than in Case I due to a larger domain, as well as a higher number of oscillations of the number of islands. On the other hand, in Case I, a larger difference between the process rate with and without capillary effects can be noticed than in Case II (X = 1.68 vs. X = 1.39).

To sum up, capillary pumping is one of the major effects observed during the membrane cleaning process at pore scale. An irregular phase boundary, with an intermediate zone, where both phases coexist, contributes to the mass transfer intensification, because the diffusion path is shorter than in the absence of capillary effects. The actual mechanism of the enhanced mass transfer comes from the convective flux in each cluster of the oil phase towards the cluster boundary, where the dissolution occurs.

3.2. Effect of the domain size and coordination number

In order to assess the role of capillary pumping in macro scale, the effect of the domain size and coordination number of the pore network on the acceleration factor X was studied. Due to the random distributions of pore and tube sizes, each simulation run yielded different results. Therefore, the values of the acceleration factor X presented below are mean values obtained for 10 simulation runs for each set of the process parameters (domain size N, domain shape factor β, coordination number n_{coord}). In Figure 7, the effect of the domain dimension on acceleration factor X is shown (2D simulations for N = 10 and 20 both with coordination number n_{coord} = 4, and 3D simulations for N = 10 with coordination number n_{coord} = 6). For the 2D simulations, the results obtained for the domains with the same shape (β = const) are very similar for N = 10 and N = 20. In both variants, the acceleration factor X equals almost 2 for a square geometry, but it decreases with increasing domain length and reaches X = 1 for β = 16 (practically no process acceleration caused by capillary pumping). On the other hand, for the 3D simulations, the process acceleration factor X increases with increasing domain size.

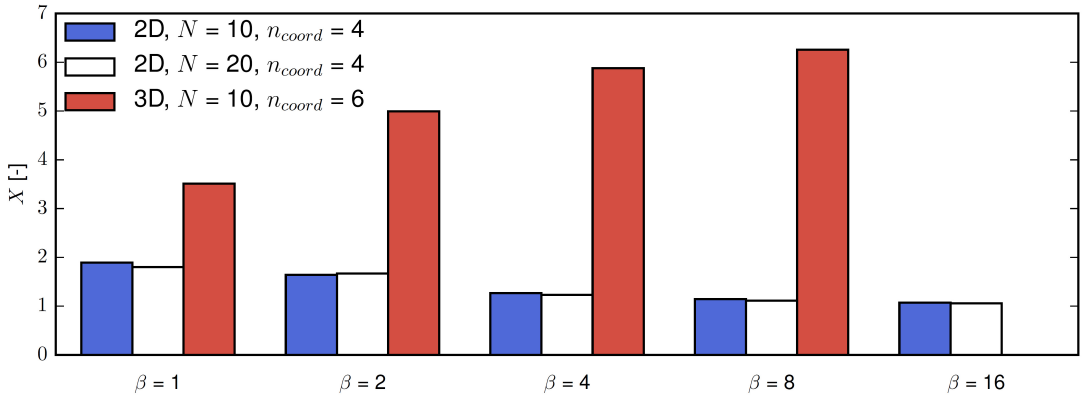

Fig. 7. Effect of domain size Non the acceleration factor X

In Figure 8, the effect of the coordination number n_{coord} of the pore network on the acceleration factor X is shown. Acceleration factors X are plotted for the following coordination number n_{coord} values: 4 (2D), 6 (3D), 8 (3D), 10 (3D), 12 (3D). As mentioned before, for the 2D simulation (n_{coord} = 4), the acceleration factor X decreases with increasing domain size and reaches 1 asymptotically. This means, that for large domains, the capillary pumping effect is not observed in macro scale. On the other hand, for all 3D simulations, the acceleration factor X increases with increasing domain size. Moreover, the acceleration effect due to capillary pumping is stronger for the pore networks with higher coordination numbers. For all

3D simulations, the process acceleration due to capillary pumping may be observed in macro scale. The main conclusion from the results presented in Figures 7 and 8 is that up to a certain critical value of the coordination number n_{coord} (less than 6), the capillary pumping effects can be observed in pore scale only, while for higher values, the effects become noticeable also in macro scale.

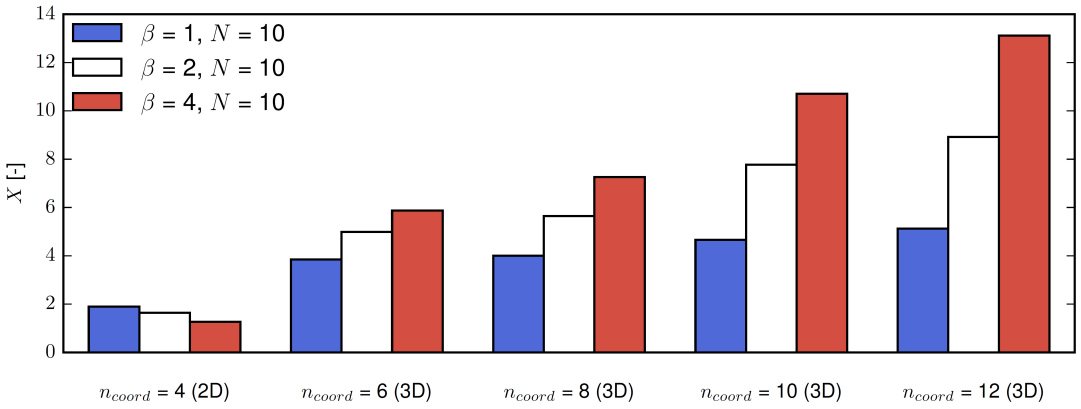

Fig. 8. Effect of the coordination number n_{coord} on the acceleration factor X

3.3. Effect of the Biot number

In the pore-scale modelling results presented above, the mass transfer resistance in the solvent flowing around the porous body was neglected. In real systems, both the convective mass transfer resistance in the bulk of the solvent and the diffusive mass transfer resistance inside the porous body contribute to the process rate. The relation between these two stages of mass transfer can be expressed by the Biot number for mass transfer:

$$\mathrm{Bi}_m = \frac{k_c L}{D} = \frac{k_c}{k_d} \tag{6}$$

where k_c is the convective mass transfer coefficient outside the porous body, L and D are the characteristic length of the diffusion path inside the porous body and the diffusion coefficient, respectively, which can be expressed as the diffusive mass transfer coefficient $k_d = D/L$. According to the expression above, Bi_m tends to infinity when the mass transfer resistance outside the porous body is neglected (like in the pore-scale simulations presented in subsections 3.1 and 3.2).

If k_d is the diffusive mass transfer coefficient in the absence of capillary effects, the effective mass transfer coefficient can be calculated by its multiplication by the acceleration factor X (calculated for $\mathrm{Bi}_m = +\infty$):

$$k'_d = X \cdot k_d \tag{7}$$

The total cleaning time is proportional to the sum of the mass transfer resistance outside and inside the porous body:

$$t\left(\mathrm{Bi}_m, X\right) \sim \frac{1}{k_c} + \frac{1}{k'_d} = \frac{1}{\mathrm{Bi}_m k_d} + \frac{1}{X \cdot k_d} \tag{8}$$

Therefore, a modified process acceleration factor X', which takes the mass transfer resistance outside the porous body into account, is a function of X and Bi_m:

$$X'\left(\mathrm{Bi}_m, X\right) = \frac{t\left(\mathrm{Bi}_m, 1\right)}{t\left(\mathrm{Bi}_m, X\right)} = X\frac{1 + \mathrm{Bi}_m}{X + \mathrm{Bi}_m} \tag{9}$$

In Table 3, the values of X' are shown as a function of X and Bi_m.

If Bi_m tends to infinity (i.e., there is no mass transfer resistance outside the porous body), X' tends to X. This means that in these conditions, process acceleration due to capillary pumping results in a proportional

Table 3. Modified process acceleration factor X'

X	Bi_m						
	0	0.1	0.3	1	3	10	$+\infty$
1	1.00	1.00	1.00	1.00	1.00	1.00	1.00
1.5	1.00	1.03	1.08	1.20	1.33	1.43	1.50
2	1.00	1.05	1.13	1.33	1.60	1.83	2.00
3	1.00	1.06	1.18	1.50	2.00	2.54	3.00
5	1.00	1.08	1.23	1.67	2.50	3.67	5.00
10	1.00	1.09	1.26	1.82	3.08	5.50	10.00

increase of the process rate. On the other hand, when Bi_m is equal to 0 (mass transfer resistance outside the porous body dominates), X' is equal to 1, and the capillary pumping effect is not observed in macro scale. For intermediate conditions ($0 < Bi_m < +\infty$), the capillary pumping effect is visible, but weaker than for $Bi_m = +\infty$. In general, the higher the mass transfer resistance in the bulk of the solvent, the lower the overall process acceleration caused by capillary pumping.

3.4. Pore-scale modelling vs. macro-scale modelling

Pore-scale modelling is useful for modelling local transport phenomena and pore-scale effects. Its application for bigger domains (up to the size of the process equipment) is limited due to high computational costs. On the other hand, although macro-scale modelling enables process simulations for the entire process apparatus, the information on the state of individual pores is not available. The pore-scale modelling results showed that the effect of pore scale phenomena (and especially the capillary pumping) on the course of the membrane cleaning process strongly depends on the coordination number of the pore network. For lower values of the coordination number ($n_{coord} < 6$), the process acceleration effect decreases with increasing computational domain. This means, that this effect is not observed at the macro scale. For higher coordination numbers of the porous structure, an inverse trend can be observed. The macro-scale model developed for the membrane cleaning process does not take into account any capillary phenomena. On the other hand, a good agreement between the simulation results and experimental results was achieved (Krzysztoforski and Henczka, 2018; Krzysztoforski et al. 2018). This suggests that in the investigated materials, the coordination number is low and, therefore, capillary pumping is effective only at pore scale, and it does not influence the course of the process at the macro scale. However, this is not a general rule and the developed model might not be accurate for the mathematical description of cleaning processes involving materials with higher coordination numbers. In this case, another macro-scale model – taking into account the pore scale effects and yielding an unsharp phase boundary – has to be used (e.g., based on the framework developed by Horgue et al. (2015)). The pore-scale model can serve as an auxiliary tool for calibration of the macro-scale model, when information on pore-scale phenomena is needed (see e.g. Attari Moghaddam et al., 2017).

4. CONCLUSIONS

The pore network study of the membrane cleaning process utilising $scCO_2$ as the cleaning fluid demonstrated that the process is characterized by the lack of a sharp phase boundary (oil phase/solvent phase), as an intermediate zone forms in the porous network, where many separate clusters (“islands”) of the oil phase

are present, surrounded by the solvent phase. This behaviour of the system leads to process acceleration caused by capillary pumping, which is a mass transfer intensification mechanism. The diffusion path is – on average – shorter than in the case when capillary effects are neglected. The effect of the domain size, the shape and the coordination number of the pore network on process acceleration was assessed. For coordination numbers lower than 6 the effect of process acceleration decreases with increasing domain size – the capillary pumping effect is limited to a small area at pore scale, and it cannot be observed at the macro scale. The analysis of the effect of the Biot number for mass transfer on the process rate shows that process acceleration weakens with the increasing mass transfer resistance of convection in the solvent flowing around the porous body. The results from this pore network study, together with experimental and numerical results from previous studies, suggest that the coordination number of the porous structure of the actual membrane used in the experimental investigation was low. However, in other systems (especially with higher coordination number values of the porous structure), capillary effects may influence the process at the macro scale. For these processes, another approach for macro-scale modelling has to be used, and the pore-scale model can be used for its calibration.

SYMBOLS

A	interfacial area, m^2
A	coefficient, s/kg
B	coefficient, s/kg
C	dimensionless concentration, –
c	concentration, g/L
D	diffusion coefficient, m^2/s
F	conductance, m^3/s
K_c	contribution coefficient, –
k_c	convective mass transfer coefficient, m/s
k_d	diffusive mass transfer coefficient, m/s
L	characteristic length, m
l	length of tube, m
m	mass, kg
$\dot{m}$	mass flux, kg/s
N	pore network size parameter, –
n_{coord}	coordination number, –
r	radius of tube, m
S	solubility of soybean oil in $scCO_2$, –
s	solubility of soybean oil in $scCO_2$, g/L
T	time, s
V_{oil}	volume of soybean oil, m^3
X	acceleration factor, –

Greek symbols

β	shape factor, –
η	cleaning efficiency, –

Subscripts

i, j	index of pores
id	ideal
m	mass

pnm pore network model
x, y, z directions in the coordinate system

ACKNOWLEDGEMENTS

Research financed by the National Science Centre, Poland, Project No. 2014/15/N/ST8/01516.

REFERENCES

Al-Dhahli A.R., Geiger S., van Dijke M.I., 2013. Three-phase pore-network modeling for reservoirs with arbitrary wettability. *SPE J.*, 18, 285–295. DOI: 10.2118/147991-PA.

Anastas P.T., Warner J.C. 1998. Principles of green chemistry, In: Anastas P.T., Warner J.C. (Eds.). *Green Chemistry: Theory and Practice*. Oxford University Press, Oxford, 29–56.

Anastas P. T., Zimmerman J.B., 2003. Peer reviewed: Design through the 12 principles of green engineering. *Environ. Sci. Technol.*, 37, 94A–101A. DOI: 10.1021/es032373g.

Attari Moghaddam A., Kharaghani A., Tsotsas E., Prat M., 2017. Kinematics in a slowly drying porous medium: Reconciliation of pore network simulations and continuum modeling. *Phys. Fluids*, 29, 022102. DOI: 10.1063/1.4975985.

Berghmans S., Berghmans H., Meijer H., 1996. Spinning of hollow porous fibres via the TIPS mechanism. *J. Membr. Sci.*, 116, 171–189. DOI: 10.1016/0376-7388(96)00037-3.

Cocero M., Alonso E., Lucas S., 2000. Pilot plant for soil remediation with supercritical CO_2 under quasi-isobaric conditions. *Ind. Eng. Chem. Res.*, 39, 4597–4602. DOI: 10.1021/ie000183y.

Horgue P., Soulaine C., Franc J., Guibert R., Debenest G., 2015. An open-source toolbox for multiphase flow in porous media. *Comput. Phys. Commun.*, 187, 217–226. DOI: 10.1016/j.cpc.2014.10.005.

Khayrat K., Jenny P., 2016. Subphase approach to model hysteretic two-phase flow in porous media. *Transp. Porous Med.*, 111, 1–25. DOI: 10.1007/s11242-015-0578-6.

Khayrat K., Jenny, P., 2017. A multi-scale network method for two-phase flow in porous media. *J. Comput. Phys.*, 342, 194–210. DOI: 10.1016/j.jcp.2017.04.023.

Krzysztoforski J., Henczka M., 2018. Porous membrane cleaning using supercritical carbon dioxide. Part 1: Experimental investigation and analysis of transport properties. *The J. Supercrit. Fluids*, 136, 12–20. DOI: 10.1016/j.supflu.2018.01.027.

Krzysztoforski J., Jenny P., Henczka, M., 2018. Porous membrane cleaning using supercritical carbon dioxide. Part 2: Development of mathematical model and CFD simulations. *J. Supercrit. Fluids*, 136, 1–11. DOI: 10.1016/j.supflu.2018.01.028.

Krzysztoforski J., Krasiński A., Henczka M., Piątkiewicz W., 2013. Enhancement of supercritical fluid extraction in membrane cleaning process by addition of organic solvents. *Chem. Process Eng.*, 34, 403–414. DOI: 10.2478/cpe-2013-0033.

Liu H., Zhu Z., Patrick W., Liu J., Lei H., Zhang L., 2020. Pore-scale numerical simulation of supercritical CO_2 migration in porous and fractured media saturated with water. *Adv. Geo-Energy Res.*, 4, 419–434. DOI: 10.46690/ager.2020.04.07.

Michałek K., Krzysztoforski J., Henczka M., da Ponte M.N., Bogel-Łukasik E., 2015. Cleaning of microfiltration membranes from industrial contaminants using “greener” alternatives in a continuous mode. *J. Supercrit. Fluids*, 102, 115–122. DOI: 10.1016/j.supflu.2015.04.011.

Özbakır Y., Erkey C., 2015. Experimental and theoretical investigation of supercritical drying of silica alcogels. *J. Supercrit. Fluids*, 98, 153–166. DOI: 10.1016/j.supflu.2014.12.001.

Rabbani A., Babaei M., Javadpour F., 2020. A triple pore network model (T-PNM) for gas flow simulation in fractured, micro-porous and meso-porous media. *Transp. Porous Med.*, 132, 707–740. DOI: 10.1007/s11242-020-01409-w.

Tarabasz K., Krzysztoforski J., Szwast M., Henczka M., 2016. Investigation of the effect of treatment with supercritical carbon dioxide on structure and properties of polypropylene microfiltration membranes. *Mater. Lett.*, 163, 54–57. DOI: 10.1016/j.matlet.2015.10.010.

Taylor M.K., Young T.M., Butzke C.E., Ebeler S.E., 2000. Supercritical fluid extraction of 2,4,6-trichloroanisole from cork stoppers. *J. Agric. Food. Chem.*, 48, 2208–2211. DOI: 10.1021/jf991045q.

Tsimpanogiannis I.N., Yortsos Y.C., Poulou S., Kanellopoulos N., Stubos A.K., 1999. Scaling theory of drying in porous media. *Phys. Rev. E*, 59, 4353. DOI: 10.1103/PhysRevE.59.4353.

Wang S., Feng Q., Javadpour F., Zha M., Cui R., 2020. Multiscale modeling of gas transport in shale matrix: an integrated study of molecular dynamics and rigid-pore-network model. *SPE J.*, 25, 1416–1442. DOI: 10.2118/187286-PA.

Xu R., Luo S., Jiang P., 2011. Pore scale numerical simulation of supercritical CO_2 injecting into porous media containing water. *Energy Procedia*, 4, 4418–4424. DOI: 10.1016/j.egypro.2011.02.395.

Yiotis A.G., Stubos A., Boudouvis A., Yortsos Y.C., 2001. A 2-D pore-network model of the drying of single-component liquids in porous media. *Adv. Water Resour.*, 24, 439–460. DOI: 10.1016/S0309-1708(00)00066-X.

APPENDIX

ALGORITHM OF THE PORE-SCALE MODEL

A.1. PORE NETWORK STRUCTURE

The pore network consists of pores and tubes. Two phases can be present inside the pores and tubes:

1) oil phase (wetting phase – soybean oil),
2) solvent phase (non-wetting phase – $scCO_2$).

The non-wetting phase is a solvent. Therefore, soybean oil can be present in this phase as a solute. The types of pores (L, A, S, G) and tubes (l, i, b, g) are listed in Table A.1 and Table A.2, respectively.

Table A.1. Types of pores

Pore type	Phases involved	Description
L	oil	The pore is completely filled with the oil phase.
A	oil+solvent	The active pore contains both phases. It is the next pore of a cluster which will be emptied.
S	solvent	The pore contains the solvent phase, but at least one neighbour pore is an L pore (connected via a b tube).
G	solvent	The pore contains the solvent phase, but none of the neighbour pores is an L pore.

Table A.2. Types of tubes

Pore type	Phases involved	Description
l	oil	The tube connects two L pores or an L pore and an A pore.
b	oil+solvent	The tube connects an L (or A) pore and an S pore. It contains the phase boundary and is a candidate for invasion, i.e., for becoming an i pore.
i	solvent	The tube leads from a G or S pore to an A pore. The respective A pore becomes invaded through this tube.
g	solvent	The tube connects two G pores.

A.2. DETAILED DESCRIPTION OF THE PORE-SCALE MODEL ALGORITHM

I. Initial stage

Preparation of computational domain and initial conditions.

a. Set pore network dimensions and topology.
b. Select boundary pores for mass transfer outlet.
c. Set all pores and tubes to G and g, respectively.
d. Set L pores in the domain (according to the initial conditions).
e. Update status of respective pores and tubes.
    i. All G pores connected to L pores become S pores.
    ii. All tubes linking two L pores become l tubes.
    iii. All tubes linking S and L pores become b tubes.

II. Time loop

1. Cluster identification step

Identification of all separate clusters of L and A pores (connected component algorithm).

2. Invasion step

Searching for new A (active) pores in each cluster.

For any cluster not containing an A pore:

i. Scan all b tubes connected to the cluster and find the one with the biggest radius (hence, with the lowest capillary pressure).
ii. The L pore, to which this b tube is leading, becomes an A pore.
iii. Update status of adjacent pores and tubes:
    A. The tube, which caused the invasion, becomes an i tube.
    B. The pore, which is connected to the i tube leading to the A pore becomes a G pore, if this pore is not connected to any b tubes.

3. Diffusion step

Solving the steady-state component balance in all non-L pores for obtaining a soybean oil concentration C distribution in the solvent phase.

i. Prepare matrix with conductance values Fi, j for each pair of neighbour pores i and j:

$$F_{i,j} = D\frac{\pi r_{i,j}^2}{l_{i,j}} \tag{A.1}$$

where D is the diffusion coefficient, and $r_{i,j}$ and $l_{i,j}$ are the radius and the length of the tube between pores i and j, respectively.

ii. Set Dirichlet pores ($C = 0$ for boundary G pores and $C = 1$ for L, A, and S pores).

iii. Calculate steady-state diffusion in the domain using a linear system solver.

4. Flux step

Calculating the mass fluxes for the clusters based on the concentration distribution from Diffusion Step.

i. Calculate all fluxes for all clusters:
Wetting phase (oil phase) balance for the A pore of each cluster:

$$\frac{\mathrm{d}V_{\mathrm{oil}}}{\mathrm{d}t} = \sum_{\text{S pores}} \sum_{\text{g tubes}} SF_{i.j}\left(C_i - C_j\right) K_c \tag{A.2}$$

where V_{oil} is the volume of the oil phase, S is the solubility of the oil in the non-wetting phase, $F_{i,j}$ is the conductance of the tube, C_i and C_j are oil concentrations in the two pores linked by the tube, and K_c is the contribution coefficient. The contribution coefficient is equal to 1, if the S pore belongs to only one cluster. Otherwise, it is calculated according to the formula below:

$$K_c = \frac{\sum_{\text{b tubes of S pore belonging to cluster}} r_{i,j}^2}{\sum_{\text{all b tubes of S pore}} r_{i,j}^2} \tag{A.3}$$

ii. Calculate cleaning times necessary to empty the corresponding A pores of all clusters.

iii. Find the minimum value of these cleaning times – the respective pore will be emptied and this cleaning time becomes the new time step.

iv. Mark the empty pore and the cluster it belongs to.

v. Update the active pore status (% filled) of the active pores of the remaining clusters.

5. Update step

Updating the status of pores and tubes of the cluster, whose pore became empty.

i. Update the status of an empty A pore: If any neighbour pore is L, the A pore becomes a S pore; otherwise, it becomes a G pore (if it was the last pore of the cluster).

ii. Update the status of tubes leading to former A pore: b and i tubes become g tubes, l tubes become b tubes.

iii. Update the status of pores connected to a former empty A pore: If the neighbour pore is not an L pore and is not connected to at least one b tube, it becomes a G pore; otherwise, it keeps its former status.

iv. If there are still any L or A pores present in the domain, go back to the beginning of the time loop. Otherwise, go to FINAL STAGE.

III. Final stage

1. Write simulation data to files.
2. Plot graphs of the simulation.

The algorithm was implemented using Python 2.6 programming language. In order to optimise the computation time, the *numpy* package was used for some data structures.

Received 07 June 2021
Received in revised form 16 August 2021
Accepted 31 August 2021